Journal of Geodesy (1999) 73: 58–66

Journal of Geodesy

© Springer-Verlag 1999

Truncated geoid and gravity inversion for one point-mass anomaly

P. Vajda[1], P. Vaníček[2]

[1] Geophysical Institute, Slovak Academy of Sciences, Dúbravská cesta 9, 842 28 Bratislava, Slovakia
e-mail: geofvajd@nic.savba.sk (cc: peter.vajda@slovnaft.sk); Tel.: +421 7 5941 0602; Fax: +421 7 375 278
[2] Department of Geodesy and Geomatics Engineering, University of New Brunswick, P.O. Box 4400, Fredericton, NB, Canada E3B 5A3
e-mail: vanicek@unb.ca; Tel.: +1 506 453 5144; Fax: +1 506 453 4943

Received: 26 September 1996 / Accepted: 28 September 1998

Abstract. The truncated geoid, defined by the truncated Stokes' integral transform, an integral convolution of gravity anomalies with the Stokes' function on a spherical cap, is often used as a mathematical tool in geoid computations via Stokes' integral to overcome computational difficulties, particularly the need to integrate over the entire boundary spheroid. The objective of this paper is to demonstrate that the truncated geoid does, besides having mathematical applications, have physical interpretation, and thus may be used in gravity inversion. A very simple model of one point-mass anomaly is chosen and a method for inverting its synthetic gravity field with the use of the truncated geoid is presented. The method of inverting the synthetic field generated by one point-mass anomaly has become fundamental for the authors' inversion studies for sets of point-mass anomalies, which are published in a separate paper. More general applications are currently under investigation. Since an inversion technique for physically meaningful mass distributions based on the truncated geoid has not yet been developed, this work is not related to any of the existing gravity inversion techniques. The inversion for one point mass is based on the onset of the so-called dimple event, which occurs in the sequence of surfaces (or profiles) of the first derivative of the truncated geoid with respect to the truncation parameter (radius of the integration cap), its only free parameter. Computing the truncated geoid at various values of the truncation parameter may be understood as spatial filtering of surface gravity data, a type of weighted spherical windowing method. Studying the change of the truncated geoid represented by its first derivative may be understood as a data enhancement method. The instant of the dimple onset is practically independent of the mass of the point anomaly and linearly dependent on its depth.

Correspondence to: P. Vajda

Key words. Gravimetric inverse problem · Truncation · Geoid interpretation · Point mass · Dimple onset

1 Introduction

The truncated geoid, defined by the Stokes' integral taken over a spherical cap rather than over the whole sphere, has been used in geodetic boundary value problem solutions as an approximation to the geoid. The truncation error (e.g. Molodenskij et al. 1962), i.e. the contribution to the Stokes' integral from the rest of the boundary, is usually estimated or modelled (de Witte 1967; Hagiwara 1972; Sjöberg 1984; Vaníček and Kleusberg 1987; Vaníček et al. 1995; Neyman et al. 1996). The truncated geoid was also used by Vaníček et al. (1987) in their comparison of marine gravity anomalies with gravity anomalies obtained from geoidal undulations derived from satellite altimetry. As such, the truncated geoid has always been associated only with a purely mathematical interpretation. We have been studying the truncated geoid as a candidate new tool in gravity inversion, motivated by its changing nature when the value of its free parameter, the radius of the integration cap (hereinafter referred to as the truncation parameter), is changed.

In spite of the gravimetric inverse problem being non-unique (e.g. Bomford 1971; Pick et al. 1973; Telford et al. 1976; Menke 1984; Moritz 1990), there is a variety of gravity field inversion techniques which invert surface gravity anomalies or disturbances of various types (using various gravity gradients, various topography or isostasy reductions, trend removal, reference field removal, spectral filtering, etc.), geoidal heights, or other quantities derived from these or from the disturbing potential, such as vertical or horizontal derivatives, etc. These techniques yield useful information on the anomalous densities producing the gravity field subject to interpretation. Methods and techniques vary with respect to the extent and depth of

the region of interest – local, regional, and global solutions – and may be classified as forward modelling, (least squares) inversion, analytical methods for restricted classes of mass distribution models, and data enhancement and display techniques. An overview of such inversion techniques may be found in e.g. Grant and West (1968), Grant (1972), Telford et al. (1976), Strakhov (1977) or Blakely (1995). Vaníček and Christou (1993) highlight the use of the geoid in gravity inversion. There are also techniques for inverting the gravity field in terms of point masses (e.g. Heikkinen 1981; Sünkel 1981, 1983; Stromeyer and Ballani 1984; Lehmann 1993). Our goal has been to develop an inversion technique using the truncated geoid. In this paper we theoretically justify the method for inverting the synthetic field of one point-mass anomaly (PMA), which was developed with the help of computer simulations. Inversion for sets of PMAs via the truncated geoid was studied next and the results are the subject of a separate paper (Vajda and Vaníček 1997).

The motivation for our investigation was the varying nature of the truncated geoid. As will be seen in the next section, the truncated geoid changes with a decreasing value of the truncation parameter from being the geoid, through being a scaled mean gravity anomaly on a region that of the cap size, to vanishing at its truncation parameter approaching zero. We studied this change as a dynamic phenomenon with respect to the truncation parameter and in terms of the anomalous mass distribution – a point mass in this particular case. By studying its change we understand studying a discrete sequence of surfaces or profiles of the first derivative of the truncated geoid with respect to the truncation parameter, whereby the value of the truncation parameter in the sequence changes systematically with a preselected step. Hereinafter we will refer to the said sequence as the derivative of the truncated geoid "(DTG) sequence". The sequence is numerically computed by direct and straightforward processing of the synthetic surface gravity (synthetic gravity anomaly) generated by the mass model (the point anomaly).

In the DTG sequence we have identified a quantifiable dynamic phenomenon, which we named the "dimple event", the onset of which is uniquely related to the depth and mass of the point anomaly. The onset of the dimple event is practically independent of the mass of the point anomaly and linearly dependent on its depth. The horizontal position of the point mass coincides with the high (positive point mass) or low (negative point mass) of the truncated geoid. The mass of the point anomaly has to be determined by an independent method, such as a least-squares method, which becomes a linear problem, once the 3-D position of the point mass is fixed (e.g. Lehmann 1993).

The above-stipulated statements originated as results of computer simulations and were proved theoretically. After defining the truncated geoid and its first derivative mathematically, we first discuss the dimple event as such and demonstrate the behaviour of its onset in response to the depth and mass of the point anomaly, and then justify it theoretically.

2 Truncated geoid and its first derivative

The truncated geoid is defined by the truncated Stokes integral (e.g. Vaníček et al. 1987)

$$N^{\psi_0}(P) = \frac{R}{4\pi\gamma} \iint_{\Re(\psi_0)} \Delta g(Q) S(P,Q)\, \mathrm{d}\sigma \tag{1}$$

The truncated geoidal height N^{ψ_0} is evaluated at the computation point P as a convolution of the gravity anomalies Δg on a spherical cap $\Re(\psi_0)$ of radius ψ_0 centered at P, with the Stokes' function S (Stokes 1849) being the convolution kernel and Q denoting the integration point. As usual, R is the radius of the boundary sphere (mean earth), γ is the normal gravity, and $\mathrm{d}\sigma$ is the surface element on the unit sphere. Integral (1) can be expressed in the local polar coordinates with the origin in P as (cf. Fig. 1)

$$N^{\psi_0}(P) = \frac{R}{4\pi\gamma} \int_0^{\psi_0} \int_0^{2\pi} \Delta g(\psi,\alpha) S(\psi) \sin(\psi)\, \mathrm{d}\psi\, \mathrm{d}\alpha \tag{2}$$

where ψ is the spherical distance between points P and Q, and α is the azimuth of point Q.

The spherical radius of ψ_0, called the truncation parameter, is a free parameter of the transformation Δg to N^{ψ_0}. Therefore the shape of the truncated geoid changes with the value of ψ_0. Indeed, for $\psi_0 = \pi$ the truncated geoid is, by definition, identical to the complete geoid. For ψ_0 approaching zero the truncated geoid vanishes:

$$\lim_{\psi_0 \to \pi} N^{\psi_0}(P) = N(P) \tag{3a}$$

$$\lim_{\psi_0 \to 0} N^{\psi_0}(P) = 0 \tag{3b}$$

The first derivative of the truncated geoid with respect to the truncation parameter (in the following, we shall call this quantity simply "the derivative", or abbreviate it as "DTG")

$$\frac{\mathrm{d}N^{\psi_0}}{\mathrm{d}\psi_0} = \lim_{\Delta\psi_0 \to 0} \frac{N^{\psi_0+\Delta\psi_0} - N^{\psi_0}}{\Delta\psi_0} \tag{4}$$

reflects the rate of change of the truncated geoid with respect to ψ_0. We wish to study this derivative since it has some very useful properties, as we will show below. To begin with, for $\psi_0 = 0$ the derivative is equal to the gravity anomaly scaled by an appropriate constant. For ψ_0 approaching π, the derivative tends to vanish:

$$\lim_{\psi_0 \to 0} \left(\frac{\mathrm{d}N^{\psi_0}}{\mathrm{d}\psi_0} \right) \Bigg|_P = \frac{R}{\gamma} \Delta g(P) \tag{5a}$$

$$\lim_{\psi_0 \to \pi} \left(\frac{\mathrm{d}N^{\psi_0}}{\mathrm{d}\psi_0} \right) \Bigg|_P = 0 \tag{5b}$$

3 Computer simulation

To study the behaviour of the truncated geoid (TG) and its derivative (DTG), we have used computer simulation.

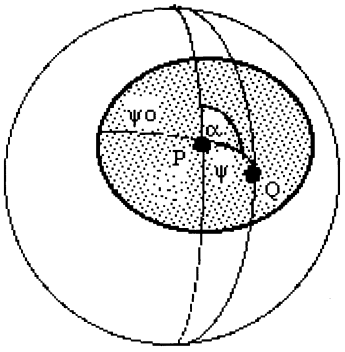

P ... computation point

Q ... integration point

ψ ... spherical distance between P and Q

α ... azimuth to Q

ψ_0 ... truncation radius, truncation parameter

Fig. 1. Truncated Stokes' integration

To begin with, we chose the simplest possible model of one PMA embedded in a sphere of constant mass density. We then let this density model generate synthetic surface gravity in terms of gravity anomalies Δg. These synthetic anomalies were then used to compute the TG and DTG sequences for uniformly decreasing values of the free parameter ψ_0.

These two sequences of surfaces, or eventually surface profiles, were then plotted to allow a visual inspection of their behaviour. The aim was to discover a quantifiable phenomenon that could be directly linked to the depth and/or the mass of the generating PMA. We succeeded in finding such a phenomenon in the DTG sequence and named it "the dimple event". The value of ψ_0, for which the dimple onset is observed, is referred to as "the instant of the dimple onset" and we denote it by ψ_0^*. In this paper we discuss how this instant is related to the depth and mass of the generating PMA.

When simulating the direct problem for one point mass, we embed the PMA of mass m at depth d in a homogeneous sphere (of mass M and radius R), representing the mean earth; see Fig. 2. The boundary sphere was chosen to be centered in the center of the total mass $M + m$, in order for the gravity field to be free of the first harmonic degree (free of forbidden harmonics). The radius R' of this sphere was selected such that the sphere is the smallest possible one that bounds all the masses.

Synthetic gravity anomalies on the boundary sphere were then generated in the following way: first the "actual" gravity on the geoid was computed from the attraction of the PMA added to the attraction of the massive sphere. The synthetic geoid was determined from the disturbing potential of the setup using the Bruns' formula. This had to be done iteratively. The normal gravity γ was generated as the attraction of a point mass $M + m$ located at the center of mass C. The normal field is thus the radial field and the normal potential and normal gravity read as follows:

$$U(Q) = \frac{\kappa(m+M)}{r}$$
$$\gamma(r = R') = \frac{\kappa(m+M)}{(R')^2} \qquad (6)$$

where κ is the gravitational constant.

The TG sequence for ψ_0 decreasing from π to 0 with a step of $\Delta\psi_0$ was computed from these synthetic gravity anomalies by numerical integration using Eq. (2). Then the corresponding DTG sequence for the same values of ψ_0 was computed by differencing the consecutive TGs and dividing the differences by $\Delta\psi_0$. Both the sequences are displayed in terms of the cross-sectional profiles running directly above the PMA in Figs. 3 and 4. As the sequences display interesting behaviour at smaller values of the truncation parameter, we show only the portion of the sequences for ψ_0 smaller than some 20°. Since the TG changes from being the geoid through being a scaled mean gravity

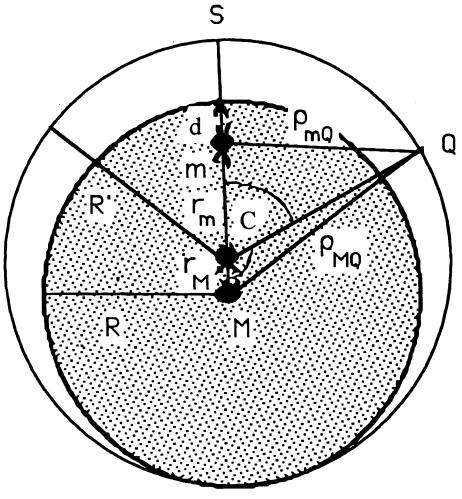

M ... center of the massive sphere
R ... radius of the massive sphere

C ... center of the boundary sphere, and center of the total mass
R' ... radius of the boundary sphere

m ... point mass

S ... projection of the point mass onto the boundary sphere
Q ... dummy point of disturbing potential, geoid, and gravity anomaly evaluation

$\psi_{SQ} = \angle(SCQ)$, $\psi_{MQ} = \angle(MCQ)$

Fig. 2. Model consisting of one PMA

anomaly until it vanishes, when decreasing ψ_0, and the DTG changes from being a scaled point gravity anomaly until it vanishes, when increasing ψ_0, cf. Eqs. (3) and (5), we choose to display the TG sequence in a decreasing and the DTG sequence in an increasing order of ψ_0 (see Figs. 3 and 4).

It is the DTG sequence that displays an interesting evolution. At first, the profile that coincides with the scaled gravity anomaly starts deforming in such a way that the feature spreads laterally while its amplitude collapses. At a certain instant, $\psi_0 = \psi_0^*$, a depression (we call it a "dimple") begins to develop in the profile. For $\psi_0 > \psi_0^*$ the dimple deepens, while the whole feature continues spreading laterally and collapsing towards zero. We refer to the value of ψ_0^* as the instant of the dimple onset. By repetitive simulations for a point mass with fixed depth and varying mass we have discovered that the value of ψ_0^* is independent of m within the accuracy of $\Delta\psi_0$ that we used. By varying the depth d of the mass anomaly we determined that ψ_0^* changes with d in a linear fashion. Since this discovery would offer interesting applications in the gravity inversion problem, we now proceed to a theoretical verification of the phenomenon.

4 Theoretical justification of the dimple

The dimple sets on right above the PMA in the DTG sequence at the instant of the curvature change of the DTG. The instant of the dimple onset ψ_0^* is therefore governed by the following equation:

$$\frac{\partial^2}{\partial\psi_{SP}^2}\left(\frac{\mathrm{d}N^{\psi_0}}{\mathrm{d}\psi_0}(\psi_0,\psi_{SP})\right)\Big|_{\psi_{SP}=0} = 0 \tag{7}$$

where ψ_{SP} is the spherical distance between the point mass location (projected onto the boundary sphere as point S) and the computation point of the DTG (point P) (cf. Figs. 2 and 5). Clearly, only $\psi_0 = \psi_0^*$ satisfies Eq. (7).

By substituting for $N^{\psi_0}(P)$ from Eq. (2) in the derivative [Eq. (7)] we obtain

$$\frac{\mathrm{d}N^{\psi_0}}{\mathrm{d}\psi_0}(P) = \frac{R}{4\pi\gamma}\int_0^{2\pi}\Delta g(\psi_0,\alpha)S(\psi_0)\sin(\psi_0)\,\mathrm{d}\alpha \tag{8}$$

and interchanging the order of the second partial derivative and the integral we arrive at

$$\int_0^{2\pi}\left(\frac{\partial^2\Delta g(\psi_0=\psi_0^*,\psi_{SP},\alpha)}{\partial\psi_{SP}^2}\Big|_{\psi_{SP}=0}\right)\mathrm{d}\alpha = 0 \tag{9}$$

The interchange is admissible, as the gravity anomalies on the boundary sphere are analytical functions.

The trivial solution $\sin(\psi_0)\,S(\psi_0) = 0$ is of no interest here (the trivial solution describes the instants when the whole DTG profile becomes zero, or in other words changes polarity, which is caused by the nodes of the Stokes' function). Thus the trivial solution is satisfied for ψ_0^* equal to 39° and 117°. Disregarding the trivial solution, Eq. (9) is the governing equation of the dimple onset.

The gravity anomalies in Eq. (9), generated by one point-mass, can be expressed by means of m, and d, of

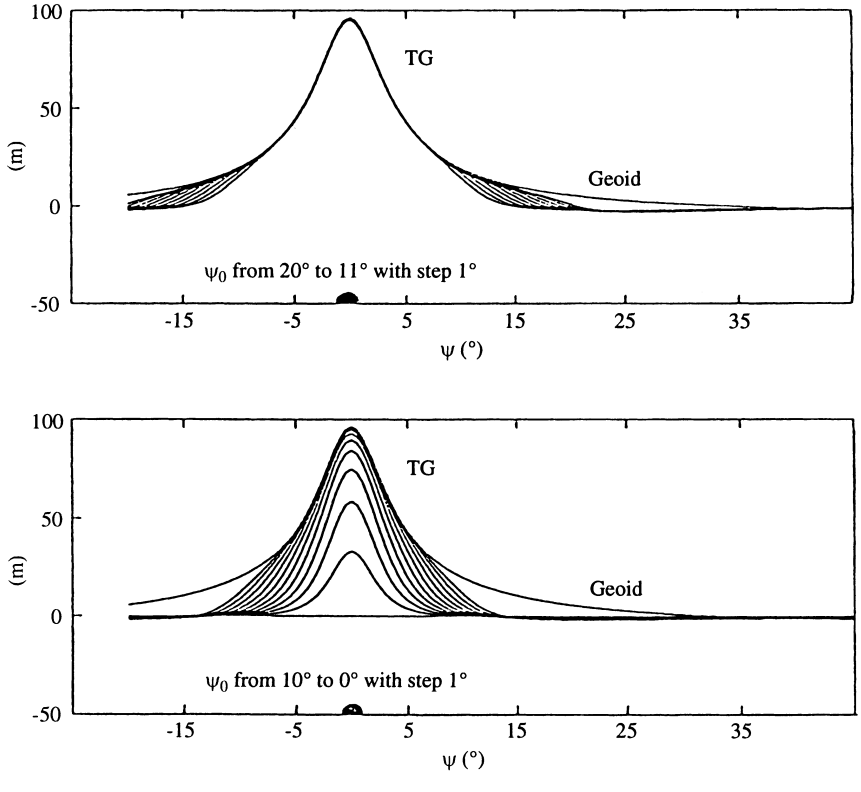

Fig. 3. The TG sequence generated by one PMA in depth $d = 319$ km producing roughly a 100-m synthetic geoid ($m/M = 8.25 \times 10^{-7}$)

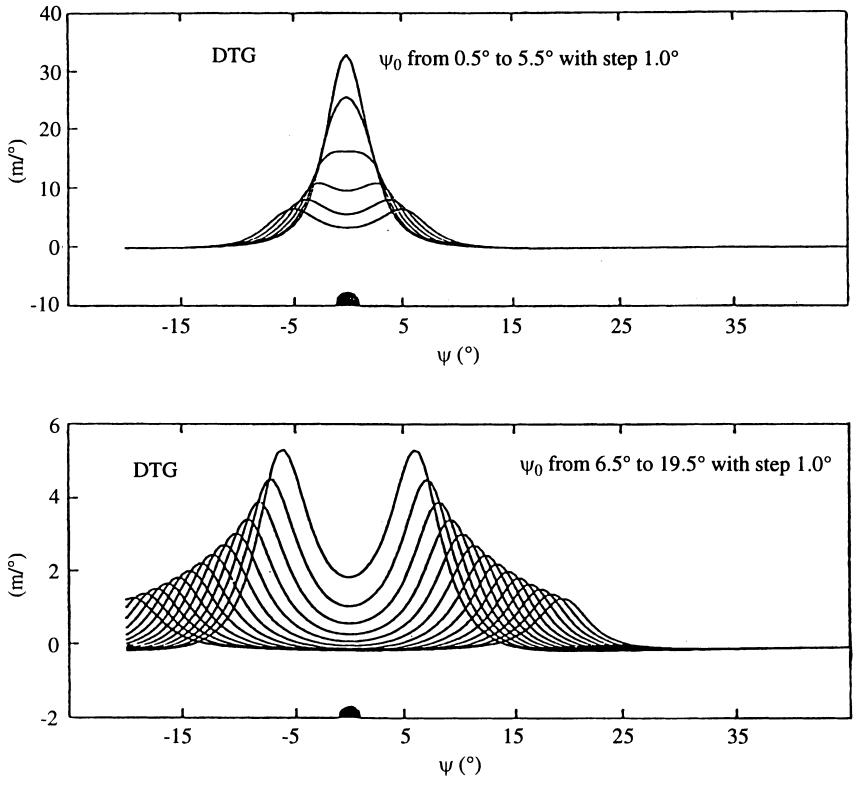

Fig. 4. The DTG sequence with respect to the TG sequence shown in Fig. 3

the point mass using the fundamental gravimetric equation (Heiskanen and Moritz, 1967)

$$\Delta g(r) = -\frac{\partial T(r)}{\partial r} + \frac{1}{\gamma}\frac{\partial \gamma}{\partial r} T(r) \tag{10}$$

where T is the disturbing potential, γ is the normal gravity, and r is the radial distance of the evaluation point Q. Thus Eqs. (9) and (10) will provide us with a functional relation between m, d and ψ_0^*. This can be done in either a spectral form, using a spherical harmonic series, or a closed analytical form.

The actual potential generated by the combination of the point mass and the massive sphere reads as (cf. Fig. 2):

$$W(Q) = \frac{\kappa m}{\rho_{mQ}} + \frac{\kappa M}{\rho_{MQ}} \tag{11}$$

with the spatial distances being given by

$$\rho_{mQ}(r = R') = \left[r_m^2 + r^2 - 2 r_m r \cos(\psi_{SQ}) \right]^{\frac{1}{2}} \Big|_{r=R'} \tag{12a}$$

$$\rho_{MQ}(r = R') = \left[r_M^2 + r^2 + 2 r_M r \cos(\psi_{SQ}) \right]^{\frac{1}{2}} \Big|_{r=R'} \tag{12b}$$

and where

$$r_m = (R - d)\frac{M}{m + M}$$
$$r_M = (R - d)\frac{m}{m + M} \tag{13}$$

$$R' = \frac{2m + M}{m + M} R - \frac{m}{m + M} d \tag{14}$$

From Fig. 5 we obtain, using spherical trigonometry

$$\cos(\psi_{SQ}) = \cos(\psi_{SP})\cos(\psi) + \sin(\psi_{SP})\sin(\psi)\cos(\alpha) \tag{15}$$

The fundamental gravimetric equation, Eq. (10), requires that the disturbing potential $[T(Q) = W(Q) - U(Q)]$ be given on the geoid. Unfortunately, we are not able to compute the actual potential on the geoid analytically, because the location (displacement with respect to the boundary sphere) of the synthetic geoid is not known to begin with. It has to be evaluated through Bruns' formula, which requires the knowledge of the disturbing potential on the geoid. We use the disturbing potential on the boundary

$$T(r = R') = \frac{\kappa m}{\rho_{mQ}}\Big|_{r=R'} + \frac{\kappa M}{\rho_{MQ}}\Big|_{r=R'} - \frac{\kappa(m + M)}{r}\Big|_{r=R'} \tag{16}$$

as an approximation to the disturbing potential on the geoid. This approximation appears acceptable when working with synthetic geoids departing from the boundary sphere by no more than 100 m. Now, by expressing the reciprocal spatial distances in Eq. (16) in Legendre polynomial series, we obtain the spectral form of the disturbing potential generated by our model on the boundary sphere as

$$T(Q) = \frac{\kappa}{R'} \sum_{n=2}^{\infty} \left[m \left(\frac{r_m}{R'} \right)^n + (-1)^n M \left(\frac{r_M}{R'} \right)^n \right] P_n(\cos(\psi_{SQ})) \tag{17}$$

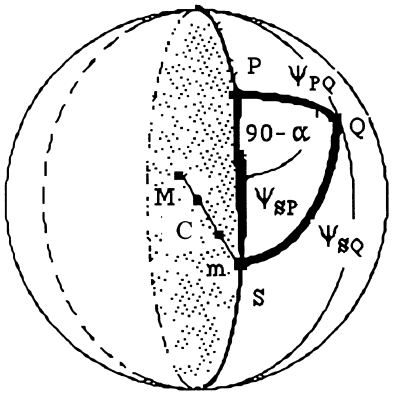

m ... position of the point mass anomaly
M ... center of the massive sphere
C ... center of the boundary sphere

S ... projection of the point mass anomaly onto the boundary sphere
Q ... dummy point of the gravity anomaly evaluation
P ... point of the truncated geoid and of its derivative evaluation

ψ ... spherical distance
α ... azimuth

Fig. 5. Geometry on the boundary sphere

where $P_n(\cos(\psi_{SQ}))$ are the Legendre polynomials.

4.1 Derivation of the instant of the dimple onset in spectral form

Substituting for the disturbing potential in Eq. (10) from Eq. (17) gives us the expression for the gravity anomalies generated by our synthetic model on the boundary sphere:

$$\Delta g(Q) = \frac{\kappa}{(R')^2}\sum_{n=2}^{\infty}(n-1) \times \left[m\left(\frac{r_m}{R'}\right)^n + (-1)^n M\left(\frac{r_M}{R'}\right)^n\right] P_n(\cos(\psi_{SQ})) \tag{18}$$

After substituting into the governing equation for the dimple onset [Eq. (9)] and performing all the necessary mathematical operations, Eq. (9) becomes

$$\sum_{n=2}^{\infty}(n-1)\left(m\left(\frac{r_m}{R'}\right)^n + (-1)^n M\left(\frac{r_M}{R'}\right)^n\right) c_n P_n(\cos(\psi_0)) = 0 \tag{19}$$

with the c_n coefficients defined as

$$c_n = -\left[\frac{\partial^2}{\partial\psi^2}P_n(\cos(\psi))\right]\Big|_{\psi=0} \tag{20}$$

and being equal to

$$c_n = \frac{\mathrm{d}P_n(\cos(\psi))}{\mathrm{d}\cos(\psi)}\Big|_{\cos(\psi)=1} = P_n'(1) \tag{21}$$

For the c_n coefficients a recurrent relation was derived based on the existing recurrent relations for Legendre polynomials (e.g. Bateman and Erdélyi 1953), which reads as follows:

$$c_n = c_{n-1} + n, \quad c_1 = 1, \quad n = 2, 3, \ldots \tag{22}$$

After taking out the multiplication factor $m\frac{r_m}{R'} = M\frac{r_M}{R'} \neq 0$ in the series of Eq. (19) and denoting the function given by such series as F, we obtain

$$F(M, R, m, d, \psi_0) \equiv \sum_{n=2}^{\infty}(n-1)\left(\left(\frac{r_m}{R'}\right)^{n-1} + (-1)^n\left(\frac{r_M}{R'}\right)^{n-1}\right) \times c_n P_n(\cos(\psi_0)) = 0 \tag{23}$$

As M and R are constant, F is an implicit function of three variables: m, d and ψ_0. We studied the convergence of the series (23) numerically and determined that, as expected, the bigger the d, and the smaller the m, the faster the convergence. An example of the function F is given in Fig. 6.

Since we are not able to rewrite the implicit function F in an explicit form in ψ_0^*, we had to resort to finding its roots $\psi_0^* = \psi_0^*(m, d)$ numerically. For this purpose we used the bisection method (Press et al. 1992). We have repeated the calculations for the depth d, varying from a few kilometres to a few thousand kilometres and for the mass m varying over several orders of magnitude, subject to the constraint that the amplitude of the generated geoid was bounded by -100 and $+100$ m. This constraint was implemented, because we wanted our model to be realistic. We found, that beside the trivial roots, the function F has two additional roots for any values of m and d. We took only the first root into consideration

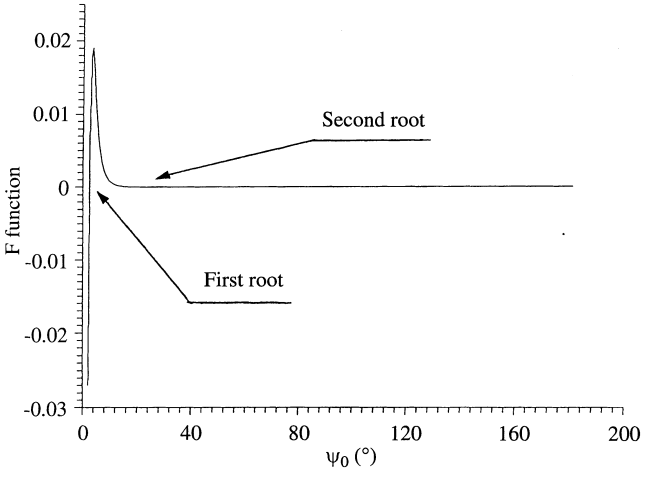

Fig. 6. An example of the function F for $d = 319$ km, and m generating roughly a 100-m synthetic geoid

for the following reason: the first root agrees with the results of the computer simulation, while the second root is very poorly determined. We suspect it to be probably an artefact caused by approximating the disturbing potential on the geoid by the disturbing potential on the boundary sphere, but we have not been able to prove this suspicion.

We found out that the dependence of the dimple onset ψ_0^* on m is very weak, while the dependence on d is strong and linear. Using the least-squares regression, we established the linear dependence to be

$$\psi_0^*[^\circ] \doteq 0.0074[^\circ/\mathrm{km}] \times d[\mathrm{km}] + \delta\psi_0^*(\mathrm{m})[^\circ] \tag{24}$$

Disregarding the weak dependence on m (i.e. the $\delta\psi_0^*(m)$ term in the above equation) causes a relative error $\delta\psi_0^*/\psi_0^*$ of only 3×10^{-5} in ψ_0^* determination. Let us have a closer look at the weak dependence of the instant of the dimple onset on the mass of the PMA. Let us rewrite Eq. (23) by splitting it into two series, and lowering the subscript n by 1, as

$$\sum_{n=1}^{\infty} n\left(\frac{r_m}{R'}\right)^n c_{n+1} P_{n+1}(\cos(\psi_0)) + \sum_{n=1}^{\infty} n(-1)^{n+1}\left(\frac{r_M}{R'}\right)^n c_{n+1} P_{n+1}(\cos(\psi_0)) = 0 \tag{25}$$

Realising that $m << M$ (m/M is actually less than 10^{-7}), we have for any n

$$\left(\frac{r_m}{R'}\right)^n >> \left(\frac{r_M}{R'}\right)^n, \quad \text{for} \quad n = 1, 2, \ldots \tag{26}$$

and we can neglect the second series with respect to the first one. Equation (25) then becomes

$$\sum_{n=1}^{\infty} n\left(\frac{r_m}{R'}\right)^n c_{n+1} P_{n+1}(\cos(\psi_0)) \doteq 0 \tag{27}$$

Since $m << M$, we can also approximate R' by R [cf. Eq. (14)] and r_m by $(R - d)$ [cf. Eq. (13)], which yields

$$\tilde{F}(M, R, \psi_0, d) \equiv \sum_{n=1}^{\infty} n\left(1 - \frac{d}{R}\right)^n c_{n+1} P_{n+1}(\cos(\psi_0)) \doteq 0 \tag{28}$$

The function $\tilde{F}$ is a special case of the function F, i.e.

$$\tilde{F}(M, R, \psi_0, d) = F(M, R, \psi_0, d, m = 0) \tag{29}$$

We have checked this derivation also numerically and established that, as expected, it gives identical numerical results for the roots $\psi_0^* = \psi_0^*(d)$ as the function F [Eq. (23)] does for the roots $\psi_0^* = \psi_0^*(m, d)$ when $m \to 0$.

4.2 Derivation of the instant of the dimple onset in a closed form

By substituting in the fundamental gravimetric equation, Eq. (9), the disturbing potential T from Eq. (17), we obtain a closed-form expression for the gravity anomalies generated by our model on the boundary sphere. Namely, we obtain

$$\Delta g(r = R') = \frac{\kappa m}{\rho_{mQ}^3}\left(R' - r_m \cos(\psi_{SQ})\right) - \frac{2}{R'}\left(\frac{\kappa m}{\rho_{mQ}} + \frac{\kappa M}{\rho_{MQ}}\right) + \frac{\kappa M}{\rho_{MQ}^3}\left(R' + r_M \cos(\psi_{SQ})\right) + \frac{\kappa(m+M)}{(R')^2} \tag{30}$$

After substituting these into the governing equation, Eq. (9), for the dimple onset and performing all the required mathematical operations, Eq. (9) becomes

$$f(m, d, \psi_0, M, R) \equiv A_1 + A_2 + A_3 + A_4 + B_1 + B_2 + B_3 + B_4 = 0 \tag{31}$$

where the A and B terms read as

$$A_1 = \frac{15 m r_m^2 (R')^2}{\rho_{m0}^7}(R' - r_m \cos(\psi_0)) \sin^2(\psi_0)$$

$$A_2 = -\frac{12 m r_m^2 R'}{\rho_{m0}^5} \sin^2(\psi_0)$$

$$A_3 = -\frac{6 m r_m R'}{\rho_{m0}^5}(R' - r_m \cos(\psi_0)) \cos(\psi_0)$$

$$A_4 = \frac{6 m r_m}{\rho_{m0}^3} \cos(\psi_0)$$

$$B_1 = \frac{15 M r_M^2 (R')^2}{\rho_{M0}^7}(R' + r_M \cos(\psi_0)) \sin^2(\psi_0)$$

$$B_2 = -\frac{12 M r_M^2 R'}{\rho_{M0}^5} \sin^2(\psi_0)$$

$$B_3 = \frac{6 M r_M R'}{\rho_{M0}^5}(R' + r_M \cos(\psi_0)) \cos(\psi_0)$$

$$B_4 = -\frac{6 M r_M}{\rho_{M0}^3} \cos(\psi_0)$$

and

$$\rho_{m0} = \left[r_m^2 + (R')^2 - 2 r_m R' \cos(\psi_0)\right]^{\frac{1}{2}}$$

$$\rho_{M0} = \left[r_M^2 + (R')^2 + 2 r_M R' \cos(\psi_0)\right]^{\frac{1}{2}}$$

Again, we were not able to rewrite Eq. (31) in an explicit form of $\psi_0^* = \psi_0^*(m, d)$ and were consigned to finding the roots of this function f numerically using the bisection method. One such function is illustrated in Fig. 7. The function f turns out to have three roots for any m and d. We only considered the first root, for the same reason as given in Sect. 4.1.

The numerical results of $\psi_0^* = \psi_0^*(m, d)$ derived from the function f display a slight distortion in the fifth

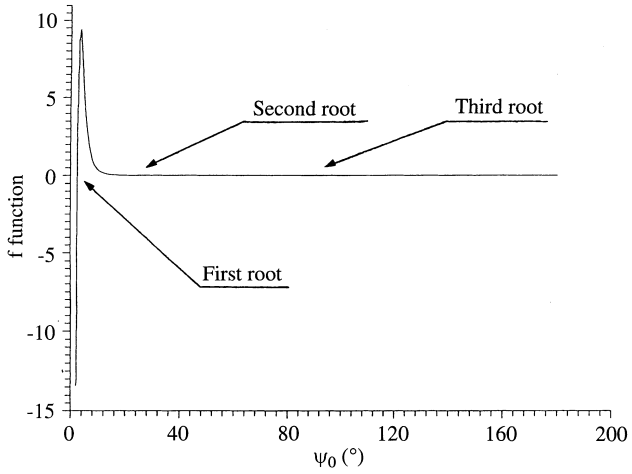

Fig. 7. An example of the f function for $d = 319$ km, and m generating roughly a 100-m geoid

decimal place of a degree compared to the results from the function F. We think that this difference can be explained by the fact that the error in ψ_0^* determination, caused by the above-discussed approximation of the disturbing potential, affects the spectral and the closed forms differently.

5 Conclusions

The theoretically derived results for the instant of the dimple onset in the DTG sequence (using a combination of analytical and numerical techniques) seem to confirm the results of computer simulation. The instant of the dimple onset ψ_0^* depends only weakly on the mass of the point anomaly and strongly on its depth, displaying a linear relation, cf. Eq. (24). Equation (24) can be inverted to give us a prescription for computing the depth d of a PMA as follows:

$$d[\mathrm{km}] = 135.82[\mathrm{km}/^\circ]\psi_0^*[^\circ] + \delta d(m)[\mathrm{km}] \qquad (32)$$

where the $\delta d(m)$ term (a function of mass m) may be neglected if we do not require relative accuracy of the depth of a PMA determination $\delta d/d$ better than 3×10^{-5}.

This means that within the above accuracy the depth of a PMA can be determined by direct processing of the surface gravity (detection of the instant of the dimple onset in the DTG sequence numerically computed from the gravity anomalies) regardless of the mass of the point anomaly, provided this point mass is the only source of the gravity anomaly.

This example of interpreting the synthetic surface gravity of one PMA in terms of the TG and DTG sequences proves that the truncated geoid also has physical applications. Suggestions as to how the introduced method could be used for inverting surface gravity fields in terms of sets of mass points are made by Vajda and Vaníček (1997). Interpretation of the truncated geoid for models more meaningful in practical geophysical or geological applications is currently under investigation.

Acknowledgements. The first author would like to acknowledge the research assistantship provided to him during his stay at the University of New Brunswick. The investigation described in this paper was part of his PhD project. The authors wish to express their thanks to Prof. L.E. Sjöberg, Prof. A. Kleusberg and Dr. Z. Martinec, who on various occasions contributed their ideas and comments to the investigations associated with this paper.

References

Bateman H, Erdélyi A (1953) Higher transcendental functions. vol. 1. McGraw-Hill, New York

Blakely RJ (1995) Potential theory in gravity and magnetic applications. Cambridge University Press, Cambridge

Bomford G (1971) Geodesy. Oxford University Press, Oxford

de Witte L (1967) Truncation errors in the Stokes and Vening Meinesz formulae for different order spherical harmonic gravity terms. Geophys J R Astr Soc 12: 449–464

Grant FS (1972) Review of data processing and interpretation methods in gravity and magnetics, 1964–71. Geophysics 37: 647–661

Grant FS, West GF (1968) Interpretation theory in applied geophysics. McGraw-Hill, New York

Hagiwara Y (1972) Truncation error formulas for the geoidal height and deflection of the vertical. Bull Géod 106: 453–466

Heikkinen M (1981) Solving the shape of the Earth by using digital density models. Rep Finnish Geod Inst 81: 2

Heiskanen WA, Moritz H (1967) Physical Geodesy. Freeman, San Fransisco

Lehmann R (1993) The method of free positioned point masses – geoid studies on the Gulf of Bothnia. Bull Géod 67: 31–40

Menke V (1984). Geophysical data analysis: discrete inverse theory. Academic Press, Orlando

Molodenskij MS, Eremeev VF, Yurkina MI (1962) Methods for the study of the external gravitational field and figure of the earth. Israel Program for Scientific Translations, Jerusalem [English translation]

Moritz H (1990) The figure of the Earth. Wichmann, Karlsruhe

Neyman YM, Li J, Liu Q (1996) Modification of Stokes and Vening–Meinesz formulas for the inner zone of arbitrary shape by minimisation of upper bound truncation errors. J Geod 70: 410–418

Pick M, Pícha J, Vyskočil V (1973) Theory of Earth′s gravity field. Elsevier, Amsterdam

Press WH, Teukolsky SA, Vetterling WT, Flannery BP (1992) Numerical recipes in FORTRAN: the art of scientific computing 2nd, edn. Cambridge University Press, Cambridge

Sjöberg LE (1984) Least squares modification of Stokes's and Vening Meinesz's formulas by accounting for the truncation and potential coefficient errors. Manuscr Geod 9: 209–229

Stokes GG (1849) On the variation of gravity at the surface of the earth. Trans Camb Philos Soc VIII: 672–695

Strakhov VN (1977) A new stage in the development of the interpretation theory of gravity and magnetic anomalies. Izvestiya, Phy Solid Earth 13: 840–852

Stromeyer D, Ballani L (1984) Uniqueness of the inverse gravimetric problem for point mass models. Manuscr Geod 9:125–136

Sünkel H (1981) Point mass models and the anomaleous gravitational field. Rep 328, Department of Geodetic Science and Surveying, The Ohio State University, Columbus

Sünkel H (1983) The generation of a mass point model from surface gravity data. Rep 353, Department of Geodetic Science and Surveying, The Ohio State University, Columbus

Telford WM, Geldart LP, Sheriff RE, Keys DA (1976) Applied geophysics. Cambridge University Press, Cambridge

Vajda P, Vaníček P (1997) On gravity inversion for point mass anomalies by means of the truncated geoid. Stud Geoph Geod 41: 329–344

Vaníček P, Christou NT (eds) (1993) Geoid and its geophysical interpretations. CRC Press, Boca Raton

Vaníček P, Kleusberg A (1987) The Canadian geoid – Stokesian approach. Manuscr Geod 12(2): 86–98

Vaníček P, Wells D, Derenyi E, Kleusberg A, Yazdani R, Arsenault T, Christou N, Mantha J, Pagiatakis S (1987) Satellite altimetry applications for marine gravity. Tech Rep 128, Department of Surveying Engineering, University of New Brunswick, Fredericton

Vaníček P, Kleusberg A, Martinec Y, Sun W, Ong P, Najafi M, Vajda P, Harrie L, Tomášek P, ter Horst B (1995) Compilation of a precise regional geoid. DSS Contract 23244-1-4405/01SS, Report for Geodetic Survey Division, Ottawa, 45 pp